European Journal of Pharmaceutics and Biopharmaceutics 142 (2019) 281–290

Contents lists available at ScienceDirect

European Journal of Pharmaceutics and Biopharmaceutics

journal homepage: www.elsevier.com/locate/ejpb

Research paper

The crucial role of macromolecular engineering, drug encapsulation and dilution on the thermoresponsiveness of UCST diblock copolymer nanoparticles used for hyperthermia

Alexandre Bordat[a], Nancy Soliman[a], Imen Ben Chraït[a], Katia Manerlax[b], Najet Yagoubi[b], Tanguy Boissenot[a], Julien Nicolas[a,*], Nicolas Tsapis[a,*]

[a] Institut Galien Paris-Sud, CNRS, Univ. Paris-Sud, Université Paris-Saclay, 92290 Châtenay-Malabry, France
[b] EA401, Matériaux et Santé, Univ. Paris-Sud, Université Paris-Saclay, 92290 Châtenay-Malabry, France

ARTICLE INFO

Keywords:
Thermoresponsive
Polymer
Nanoparticles
UCST
Doxorubicin
Hyperthermia

ABSTRACT

Poly(acrylamide-co-acrylonitrile) (P(AAm-co-AN)), an upper critical solution temperature (UCST)-type copolymer in water, was synthesized by reversible addition fragmentation chain transfer (RAFT) copolymerization and used as a macro-RAFT agent for the polymerization of oligo(ethylene glycol) methyl ether methacrylate (OEGMA) to yield amphiphilic diblock P(AAm-co-AN)-b-POEGMA copolymer. A series of copolymers with different AN content was obtained allowing to finely tune the UCST behavior (cloud point ($T_{t\text{-}UCST}$) from 35 to 78 °C). Addition of the POEGMA block did not modify the $T_{t\text{-}UCST}$ regardless its Mn but provided a lower critical solution temperature behavior at high temperature. Nanoparticles were then formulated by the nanoprecipitation technique revealing that copolymers with higher $T_{t\text{-}UCST}$ yield smaller, better-defined nanoparticles. Eventually, doxorubicin (Dox) was encapsulated into nanoparticles made from the copolymer having a $T_{t\text{-}UCST}$ close to mild hyperthermia (~43 °C). Surprisingly, Dox encapsulation increased $T_{t\text{-}UCST}$ and gave smaller nanoparticles as opposed to their unloaded counterparts. The dilution of the suspension also led to a decrease of Tt-UCST. No obvious hyperthermia effect was observed on the cytotoxicity of Dox-loaded nanoparticles. Our study highlighted the influence of macromolecular engineering, drug encapsulation and nanoparticle dilution on UCST behavior, important features often overlooked despite their crucial impact in the development of thermosensitive nanoscale drug delivery systems.

1. Introduction

Nanomedicine holds great promise in dealing with the shortcomings of fragile and/or poorly soluble anticancer drug formulations, such as longer circulation time [1] and fewer side effects for the healthy tissues [2]. Newer generations of nanoparticles aim at going one step further by allowing full control of the spatial and temporal release of the drug. This is made possible by, for instance, employing stimulus-responsive starting material to build the drug carrier [3]. Temperature is an easy-to-use trigger that can be exploited through mild hyperthermia, corresponding to an elevation of tissue temperature from 37 °C to 43 °C [4]. Clinicians dispose of a wide array of tools to locally heat tissue, such as ultrasound [5], microwave [6], radiofrequency [7] and infrared [8] energy sources. Mild hyperthermia has a biological effect on the tumor microenvironment as the endothelial tissue becomes more permeable [9,10] and immune response is enhanced [11,12]. Thus, the prospect of using mild-hyperthermia with tailored nanomedicine is enthralling and should lead to better disease management [13]. To the best of our knowledge, only one thermoresponsive formulation of doxorubicin (Dox) exists in clinical stages of development. It is in the form of thermosensitive liposomes that are currently undergoing phase 3 of clinical trials, under the name of ThermoDox® by Celsion [14]. ThermoDox® is intended to work as a companion for radiofrequency tumor ablation. It is administered intravenously while the tumor is being ablated by radiofrequency. The generated heat triggers the local release of Dox that in turn exerts its effect on the remaining tumor cells that were not fully ablated by radiofrequency. Although the formulation is in clinical trials, there are still some limitations regarding this system as liposomes are fragile and have poor drug retention [15,16].

In contrast, polymer nanoparticles may provide better drug retention and in terms of polymer chemistry, there is still no thermoresponsive polymer nanoparticle formulation undergoing clinical trials.

* Corresponding authors.
E-mail addresses: julien.nicolas@u-psud.fr (J. Nicolas), nicolas.tsapis@u-psud.fr (N. Tsapis).

https://doi.org/10.1016/j.ejpb.2019.07.001
Received 30 April 2019; Received in revised form 27 June 2019; Accepted 1 July 2019
Available online 04 July 2019
0939-6411/

Lower critical solution temperature (LCST) thermoreponsive polymers have been used to produce thermoresponsive nanocarriers for several decades [17], but yet without successful translation to the clinic [18]. These polymers are soluble in water below the LCST and insoluble above. On the other hand, upper critical solution temperature (UCST) polymers are less widely investigated while their thermoresponsiveness appears more intuitive as they are fully soluble above the UCST and insoluble below. An example of such polymer is poly(acrylamide-*co*-acrylonitrile) (P(AAm-*co*-AN)) [19], a UCST-type copolymer that owes its thermoresponsiveness to the reversible hydrogen bonds made between the copolymer chains below the UCST and the surrounding water molecules above the UCST. In terms of polymer synthesis, P(AAm-*co*-AN) can be easily synthesized by free-radical polymerization [19–21] or reversible deactivation radical polymerization techniques such as reversible addition fragmentation chain transfer (RAFT) polymerization [22–26]. The copolymer obtained by free-radical polymerization has been grafted with poly(ethylene glycol) (PEG) on the acrylamide monomers to formulate thermoresponsive nanoparticles efficiently responding to mild-hyperthermia for in vivo tumor treatment [27].

Here, we design a different synthetic route to yield a well-defined, amphiphilic block copolymer. A poly(acrylamide-*co*-acrylonitrile)-*b*-poly[(oligo(ethylene glycol) methyl ether methacrylate)] (P(AAm-*co*-AN)-*b*-POEGMA) diblock copolymer was synthesized by RAFT polymerization of OEGMA from a P(AAm-*co*-AN) UCST-type macro-RAFT agent. This strategy allowed control on the size of both the thermoresponsive block and the hydrophilic block. Copolymers with different M_n and AN content were synthesized to optimize the cloud point ($T_{t\text{-}UCST}$) for mild hyperthermia. These copolymers were then formulated into nanoparticles and the influence of the $T_{t\text{-}UCST}$ on the physico-chemical properties of the colloidal suspension was investigated. We also evaluated the effect of Dox encapsulation on nanoparticle thermoresponsiveness and characteristics, as the influence of drug encapsulation is often overlooked despite its crucial impact in the development of thermosensitive nanoscale drug delivery systems. Finally, Dox-loaded nanoparticle cytotoxicity was assessed in vitro on ovarian cancer cells with or without application of hyperthermia.

2. Materials and methods

2.1. Materials

Acrylamide (AAm) (Sigma-Aldrich) was recrystallized in chloroform, acrylonitrile (AN) (Sigma-Aldrich) was purified by passing through a column filled with activated, basic, Brockman I aluminum oxide. Azobisisobutyronitrile (Sigma-Aldrich) was recrystallized in ethanol. Oligo(ethylene glycol) methyl ether methacrylate (OEGMA) ($M_n \sim 300$ g mol^{-1}, Sigma-Aldrich), 2-cyano-2-propyl benzodithioate (CPDB) (Sigma-Aldrich), doxorubicin hydrochloride (Dox.HCl) (Carbosynth), and triethylamine (TEA) (Sigma-Aldrich) were used as received. RPMI-1640 cell culture medium and bovine insulin were purchased from Sigma-Aldrich. Water was purified using a MilliQ Reference system from Merck-Millipore. Solvents were of HPLC analytical grade and were provided by Carlo Erba (Italy). For NMR measurements, d_6-DMSO was provided by Eurisotop (France).

2.2. Fourier transform infrared (FTIR) spectroscopy for AN quantification

KBr pellets containing the polymer samples were prepared for transmission FTIR analysis using FTIR Spectrum One (PerkinElmer) by mixing polymer samples with KBr at 5 wt% and running 5 scans at 4 cm^{-1} resolution per sample. For mol.% AN determination, a calibration curve was obtained by mixing PAAm and PAN (both from Sigma-Aldrich) at determined ratios and by calculating the peak area ratio between the carbonyl peak (C═O at 1659 cm^{-1}) and the nitrile peak (C≡N at 2242 cm^{-1}) (Supplementary Information, Fig. S7). Experiments were performed at least in six replicates.

2.3. Nuclear magnetic resonance (NMR) spectroscopy

^{1}H NMR spectroscopy was performed in 5 mm diameter tubes in d_6-DMSO at 70 °C for 128 scans on a Bruker Avance 3 HD 400 spectrometer at 400 MHz. NMR determination of the M_n of P(AAm-*co*-AN) copolymers was achieved by integrating the triplet between 7.88 and 7.98 ppm corresponding to 2 aromatic protons from the CPDB end-chain (noted *a* in Supplementary Information, Fig. S1) and the broad peak between 1.40 and 2.09 ppm assigned to the protons of the methylene group in all monomer units (noted *g* in Supplementary Information, Fig. S1), that allowed determination of the total content in AAm and AN. By using the measured mol.% AN using method 2.2., the M_n was then determined. For P(AAm-*co*-AN)-*b*-POEGMA copolymers, integration of the broad peak between 6.25 and 7.75 ppm corresponding to the NH_2 protons of the acrylamide, was compared to the integration of the peak between 3.95 and 4.18 ppm corresponding to 2 OEGMA protons (Supplementary Information, Fig. S1).

2.4. Size exclusion chromatography (SEC)

SEC was performed at 50 °C with two columns from PSS Gram (GPC column 300 × 8 mm; bead diameter 10 μm; molar mass range 500–10^6 g.mol^{-1}) and a triple detection system (Viscotek TDA/GPCmax from Malvern) with a differential refractive index detector, low and right-angle light scattering detectors and a differential viscometer detector. The eluent was dimethyl sulfoxide (DMSO) at a flow rate of 0.7 mL min^{-1}. The system was calibrated using a narrow pullulan standard and each polymer sample was injected at 5 different injection volumes for the determination of the *dn*/*dc* parameter. This allowed the determination of the number-average molar mass (M_n), the weight-average molar mass (M_w) and the dispersity ($Đ = M_w/M_n$).

2.5. Suspension turbidity for $T_{t\text{-}UCST}$ and $T_{t\text{-}LCST}$ determination

Light transmittance (%) of samples was measured using a Lambda 25 UV/VIS spectrometer equipped with a PTP 1 + 1 Peltier system for temperature control (PerkinElmer). Samples were prepared at 4.5 mg mL^{-1}, spectrometer wavelength was set at 600 nm, temperature ramp was at 0.5 °C min^{-1} and data acquisition was performed every 30 s. The transition temperature $T_{t\text{-}UCST}$ is defined as the point at which the transmittance reaches a maximum plateau for UCST behavior. For LCST behavior Tt-LCST corresponds to the point at which the transmittance reaches a minimum plateau. Experiments were performed at least in duplicates.

2.6. Dynamic light scattering (DLS) and zeta potential

Nanoparticle intensity-averaged diameters (D_z) and zeta potentials (ζ) were measured by dynamic light scattering (DLS) with a Nano ZS from Malvern (173° scattering angle) at a temperature of 20 °C. The surface charge of the nanoparticles was investigated by ζ-potential (mV) measurement at 20 °C after dilution with 1 mM NaCl, using the Smoluchowski equation. Experiments were performed at least in triplicate.

2.7. UV spectroscopy for doxorubicin quantification

3 mL of the suspension were centrifuged at 20,000*g* for 1 h at 4 °C (Optima LE-80K Ultracentrifuge Beckman Coulter). The supernatant was discarded, and the pellet was dissolved in 5 mL of DMSO. The dissolved samples were put in 96-well plates before quantification at 490 nm by a plate reader. Calibration curve was determined by preparing a solution of Dox at 6 mgmL^{-1} and TEA (35 μL) in DMSO and subsequent dilution to a range between 6 and 200 μg mL^{-1} of Dox. Drug loading (DL, wt.%) and encapsulation efficiency (EE, wt.%) were calculated using the following formulas:

$$DL = \frac{mass\ of\ encapsulated\ Dox}{mass\ of\ encapsulated\ Dox + mass\ of\ polymer} \times 100$$

$$EE = \frac{mass\ of\ encapsulated\ Dox}{mass\ of\ initial\ Dox} \times 100$$

Experiments were performed in triplicate.

2.8. Transmission electron microscopy (TEM)

TEM images were obtained using transmission electron microscope of 80 kV Jeol 1400 (Imagif, I2BC, CNRS, Gif-sur-Yvette, France). Briefly, each suspension was diluted ten-fold in water. Then, 3 µL of this dilution were placed on a glow-discharged copper grid covered with formvar-carbon film. The excess solution was blotted off using a filter paper. Images were acquired using an Orius camera (Gatan Inc, USA).

2.9. Synthesis of P(AAm-co-AN)

The overall procedure was adapted from the work of Zhang et al. [22] Proportions were changed according to the desired polymer composition. A typical synthesis (**T2**) is as follows: AIBN (2.3 mg, 0.014 mmol), CPDB (15.7 mg, 0.071 mmol), AAm (3.324 g, 46.76 mmol), AN (0.918 g, 17.29 mmol) and DMSO (16.01 mL) were charged in a 50 mL-round-bottom flask. For other copolymer compositions, see details in Supplementary Information (Table S2). The mixture was purged with argon for 15 min under vigorous stirring before being placed in a 70 °C-oil bath for 24 h under stirring. After the reaction, the copolymer was precipitated twice in methanol (20 times the volume of the mixture). The copolymer was further solubilized in DMSO and placed in a 3.5 kD Spectra/Por 3 dialysis bag for dialysis against water for 3 days at room temperature (20 °C), with dialysis water changed twice per day. The dialysate was then freeze-dried to yield P(AAm-*co*-AN) as a red hard solid paste.

2.10. Synthesis of P(AAm-co-AN)-b-POEGMA

P(AAm-*co*-AN) was used as a macro-RAFT agent to polymerize OEGMA and yield a P(AAm-*co*-AN)-*b*-POEGMA diblock copolymer. An example of synthesis as follows: P(AAm-*co*-AN) (**T2**) (200 mg, 6.25 µmol), OEGMA (75 mg, 250 µmol), AIBN (1.7 mg, 10.4 µmol) and DMSO (4.5 mL) were charged in a 20 mL-vial. The mixture was purged with argon for 15 min under vigorous stirring before being placed in a 70 °C-oil bath for 5 h under stirring. The mixture was directly put into a 3.5 kD Spectra/Por 3 dialysis bag for dialysis against water for 24 h, with dialysis water changed three times. The dialysate was then freeze-dried to yield the diblock copolymer as a white-reddish soft solid paste.

2.11. Unloaded nanoparticle formulation

Preparation of thermoresponsive copolymer nanoparticles was carried out using the nanoprecipitation technique. 50 mg of copolymer were dissolved in 1 mL of DMSO. The solution was added at 150 µL/min using a syringe pump (Harvard Apparatus Pump 11 Pico Plus Elite) to 10 mL of water (or PBS 0.01 M containing 0.15 M NaCl) under vigorous stirring. To remove DMSO, the suspension was put into a 3.5 kD Spectra/Por 3 dialysis bag for dialysis against water (or PBS) for 24 h, with dialysis medium changed twice.

2.12. Doxorubicin-loaded nanoparticle formulation

The protocol was adapted from Huang et al. [23] and is described as follows: 50 mg of copolymer were dissolved in 500 µL of DMSO. Dox.HCl (5 mg, 8.62 µmol) was dissolved in 500 µL of DMSO prior to addition of 35 µL (251 µmol) of TEA and the solution was stirred for 7 h shaded from light at room temperature. The copolymer and Dox solutions were then mixed, and the following steps were the same as in Section 2.11 in water only, with the solutions shaded from light. For the drug encapsulation curve, the amount of initial Dox.HCl varied from 1 to 5 mg.

2.13. Cell culture

Nanoparticle cytotoxicity was evaluated on the human ovarian carcinoma cell line OVCAR-3 obtained from ATCC (USA). OVCAR-3 cells were cultured in RPMI-1640 medium supplemented with 100 U/mL penicillin, 20% heat inactivated FBS, and 0.01 mg.mL^{-1} bovine insulin. The cell line was maintained at 37 °C and 5% CO_2 in a humidified atmosphere and cells were split twice weekly. The cell viability was evaluated using the 3-[4,5-dimethylthiazol-2-yl]-3,5-diphenyltetrazolium bromide (MTT) assay. Briefly, cells were seeded in 100 µL of culture medium (8×10^3 cells/well for 72 h incubation) in 96 well plates (TPP, Switzerland) and pre-incubated for 24 h. 100 µL of a serial dilution of nanoparticle suspension was then added to the medium. After 72 h of incubation, 20 µL of MTT solution (5 mg.mL^{-1} in PBS) was added to each well. After 4 h incubation, the culture medium was gently aspirated and replaced by 200 µL DMSO (ACS grade, VWR, France) to dissolve the formazan crystals. The absorbance of the solubilized dye, which correlates with the number of living cells, was measured with a microplate reader (LAB Systems Original Multiscan MS, Finland) at 570 nm. The percentage of viable cells in each well was calculated as the absorbance ratio between nanoparticle-treated and untreated control cells. For hyperthermia studies, the protocol was the same except cells were incubated at 43 °C for 30 min, either 6 h or 24 h after nanoparticle addition to the wells. After 30 min, the cells were put back in the incubator at 37 °C until they had been exposed for a total of 72 h. Experiments were performed in triplicate. Data was fitted to a Hill slope model with four parameters using GraphPad Prism 7 which allowed determination of the IC_{50} for the Dox-containing treatments. The different IC_{50} values were compared using a one-way ANOVA test with GraphPad Prism 7.

3. Results and discussion

3.1. Thermoresponsive copolymer synthesis and UCST behavior

Thermoresponsive poly(acrylamide-*co*-acrylonitrile) (P(AAm-*co*-AN)) copolymers with different AN contents were synthesized to evaluate the dependency of the UCST behavior relative to the AN content (Fig. 1, T1–T8, Table 1). Among the different reversible deactivation radical polymerization techniques, RAFT polymerization was chosen for its simplicity, its ability to control such monomers, together with its capability to form well-defined block copolymers by efficient chain-extension from macro-RAFT agents (Fig. 1) [28–31]. AN content was determined by infrared spectroscopy against a pre-determined calibration curve (Supporting Information, Fig. S7). AN content was in good correlation with the theoretical value, yet the technique was not completely robust as values for **T4** and **T8** had an important standard deviation and it proved difficult to get a good measurement for **T3**. After synthesis of the P(AAm-*co*-AN) block, our approach consisted in performing its chain-extension by polymerizing oligo(ethylene glycol) methyl ether methacrylate (OEGMA, $M_n \sim 300$ g mol^{-1}) under RAFT control to yield the corresponding P(AAm-*co*-AN)-*b*-POEGMA diblock copolymer comprising a thermoresponsive UCST-type block and a hydrophilic one (Fig. 1, P1 – P8, Table 2). Importantly, the hydrophilic POEGMA block acts as a biocompatible and protein repellent corona to prolong the blood circulation time of the nanoparticles (the so-called "stealth" feature) [32,33]. The M_n of the different copolymers was measured both by ^{1}H NMR and a triple detection SEC (that allows absolute M_n values to be determined). Even though SEC is the most used method for M_n determination, ^{1}H NMR is appealing as integration of chain-end protons allows precise M_n measurement (irrespectively of the

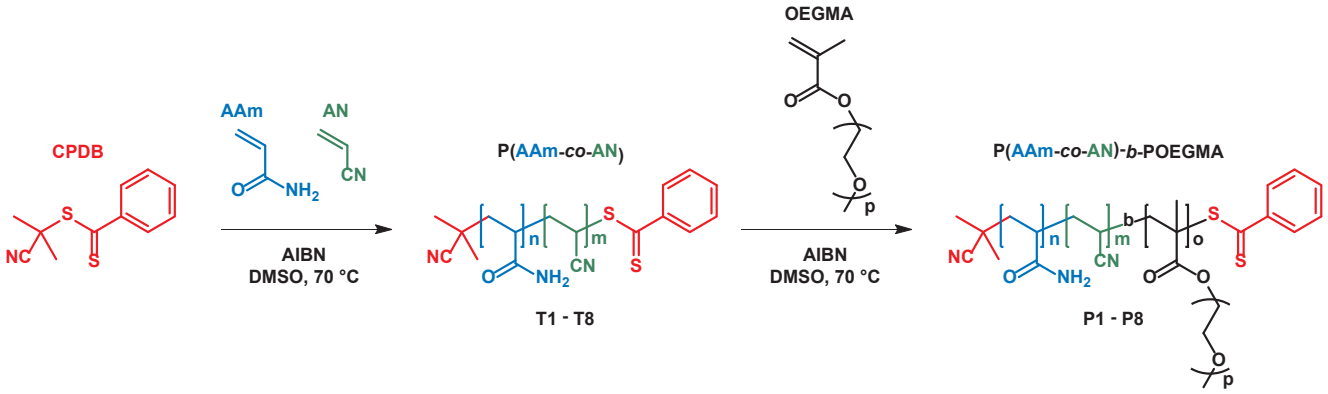

Fig. 1. Synthesis of a series of UCST thermoresponsive poly(acrylamide-co-acrylonitrile), P(AAm-co-AN), copolymers (T1 – T8, Table 1) used as macro-RAFT agents to yield poly(acrylamide-co-acrylonitrile)-b-poly[(oligo(ethylene glycol) methyl ether methacrylate)] (P(AAm-co-AN)-b-POEGMA) diblock copolymers (P1 – P8, Table 2).

Table 1
Characterization of the different thermoresponsive P(AAm-co-AN) copolymers synthesized in this study. AN content determined by IR spectroscopy, value given with SD. $M_{n\text{-}NMR}$ calculated by ^{1}H NMR in d_6-DMSO. *: sample was difficult to process into KBr pellets and measured value was out of calibration range. ins.: insoluble in water at any temperature.

Sample	AN in feed (mol.%)	AN in polymer (mol.%)	$M_{n,NMR}$ (g mol^{-1})
T1	25	28 ± 0.5	34,400
T2	27	30.1 ± 2.5	31,700
T3	28	–*	32,700
T4	30	33.4 ± 9.1	44,800
T5	31	29.6 ± 1.6	29,500
T6	33	32.6 ± 1.8	36,000
T7	35	35.5 ± 2.7	42,400
T8	40	40.4 ± 4.4	20,700

Table 2
Characterization of the different thermoresponsive P(AAm-*co*-AN)-*b*-POEGMA diblock copolymers synthesized in this study. $M_{n\text{-}NMR}$ calculated by ^{1}H NMR in d_6 -DMSO. $M_{n\text{-}SEC}$ determined by triple detection SEC in DMSO. $Đ$ is polymer dispersity. T_t determined by UV-vis temperature ramp at 4.5 mg.mL^{-1} in PBS. ins.: insoluble in water at any temperature. SEC chromatograms of P1-P8 are presented in Supplementary Information (Fig. S3).

Sample	POEGMA block $M_{n,NMR}$ (g mol^{-1})	Diblock $M_{n,NMR}$ (g mol^{-1})	Diblock $M_{n,SEC}$ (g mol^{-1})	$Đ$	T_t (°C)
P1	16,300	50,700	48,700	1.19	35
P2	8,500	40,200	41,100	1.17	47
P3b	9,400	42,100	38,800	1.14	50
P4	26,000	70,800	63,200	1.11	61
P5	15,000	44,500	36,000	1.11	66
P6	21,100	57,100	45,500	1.10	74
P7	42,300	84,700	56,900	1.15	78
P8	4,100	24,800	20,500	1.13	ins.

nature of the polymer), providing the M_n is rather low. In our case, since we have synthesized relatively large copolymers ($M_{n,SEC}$ = 20–63 kg mol^{-1}), some discrepancies were observed between, $M_{n,SEC}$ and $M_{n,NMR}$ (Fig. 1, Tables 1 and 2). Overall, well-defined copolymers were obtained with dispersity values below 1.2 for both the thermoresponsive block and the diblock copolymers. Copolymers **P1** to **P7** were soluble in DMSO or in hot water (above their T_t, up to 80 °C), whereas **P8** was only soluble in DMSO. These results indicate that ~40 mol.% AN is too high for hyperthermia as it yielded a water-insoluble copolymer with an out-of-range UCST value (> 100 °C).

The influence of PEGylation on the thermoresponsiveness of the P(AAm-*co*-AN) block was then investigated. Addition of the POEGMA block had no impact on the $T_{t\text{-}UCST}$, as shown with **T3** and **P3a – P3c**

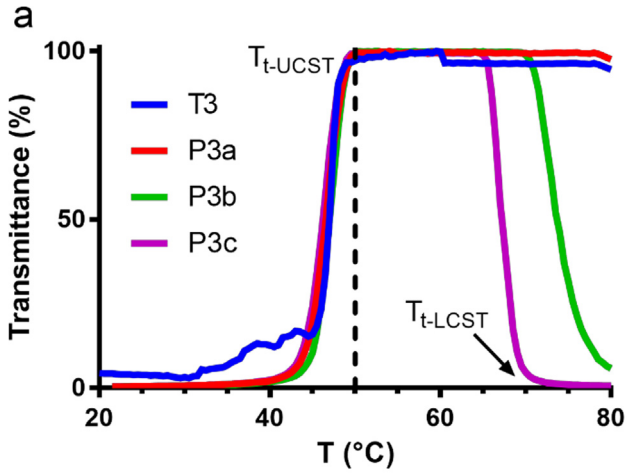

b Sample	M_n POEGMA (g.mol^{-1})	$T_{t\text{-}UCST}$ (°C)	$T_{t\text{-}LCST}$ (°C)
T3	0	50	n.m.
P3a	4,900	50	n.m.
P3b	9,400	50	80
P3c	22,400	50	70

Fig. 2. (a) Thermoresponsive properties (transmittance curves, 4.5 mg mL^{-1} in water) of P(AAm-*co*-AN) **T3** and P(AAm-*co*-AN)-*b*-POEGMA diblock copolymers of different M_n **P3a** to **P3c**. (b) $T_{t\text{-}UCST}$ and $T_{t\text{-}LCST}$ values of the synthesized copolymers. M_n was calculated by ^{1}H NMR, $T_{t\text{-}LCST}$ is the temperature at which the transmittance reaches a minimum plateau, n.m.: not measurable. SEC chromatograms are presented in Supplementary Information (Fig. S3).

(Fig. 2a) until a certain chain length where POEGMA exhibited a LCST [34] behavior that was influenced by its M_n (Fig. 2b). Despite the increasing M_n of the hydrophilic POEGMA blocks added to **T3**, from 4900 g mol^{-1} to 22,400 g mol^{-1}, it did not prevent the diblock copolymers to retain their thermoresponsiveness. This is true even for **P7**, having a M_n composed 50% by the thermoresponsive block and 50% by the hydrophilic block, which retained its UCST properties. Importantly, the $T_{t\text{-}LCST}$ values of **T3**-based thermosensitive diblock copolymers were all ≥70 °C, which is much higher than mild-hyperthermia (43 °C) and should not hamper the mild-hyperthermia-mediated drug release.

Since these copolymers are intended for use in a biological setting, we have evaluated the influence of the presence of electrolytes on their UCST behavior in water and in PBS. For **P2**, we observed that the copolymer in water did not exhibit a marked hysteresis and the heating and cooling $T_{t\text{-}UCST}$ were nearly identical (Supplementary Information Fig. S4a). The effect of ionic strength and pH was then assessed by

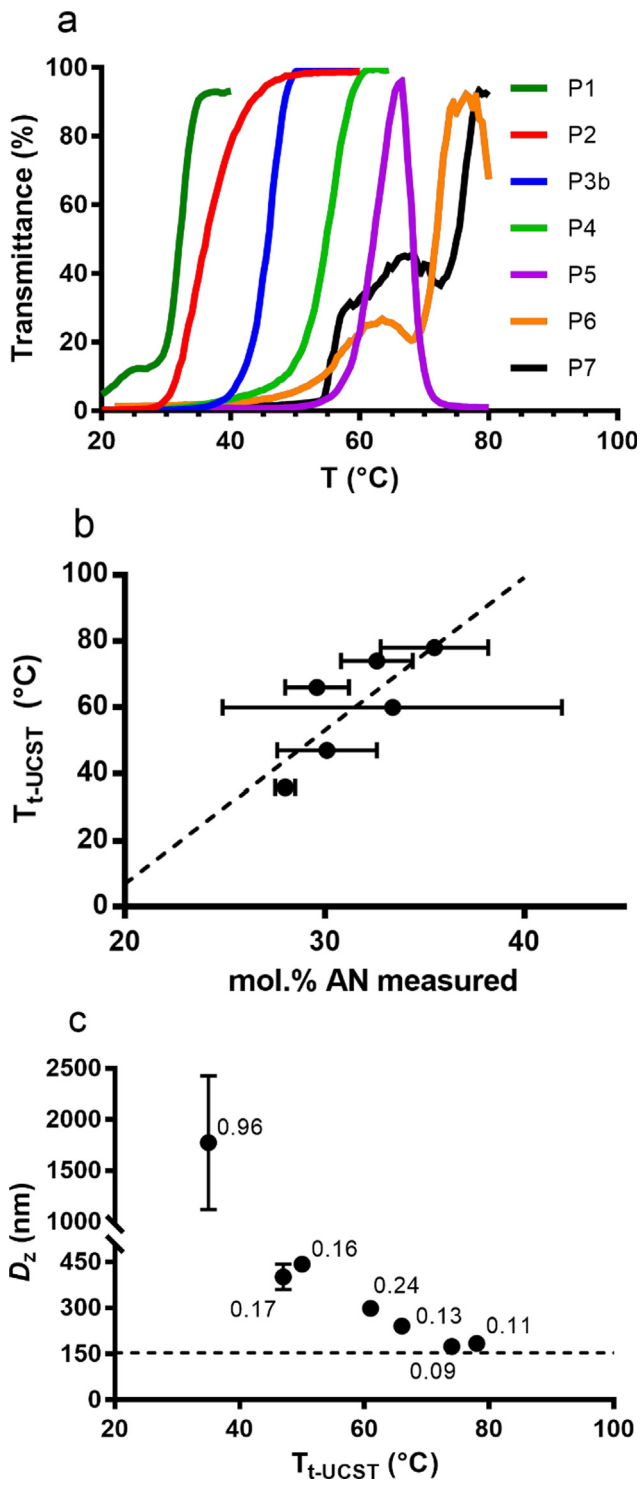

Fig. 3. Heating transmittance curves of the different polymers at 4.5 mg mL^{-1} in PBS (a) and $T_{t\text{-}UCST}$ plotted against the measured AN mol.% content (b). Intensity-averaged diameter (D_z) and polydispersity index (PdI) in water measured by DLS of P(AAm-*co*-AN)-*b*-POEGMA diblock copolymers nanoparticles as a function of the $T_{t\text{-}UCST}$ (c). The tags on each data point correspond to the polydispersity index (PdI). The line at 154 nm represents the D_z of nanoparticles obtained with the non-thermoresponsive polymer **P8** (PdI = 0.05). For each sample n ≥ 3.

measuring the $T_{t\text{-}UCST}$ in PBS. The hysteresis is here more pronounced compared to that obtained in water (Supplementary Information Fig. S4b). When comparing the heating and cooling curves in water and PBS, $T_{t\text{-}UCST}$ remained constant at 47 °C in both media, but the thermoresponsiveness onset for the heating curve occurred earlier in PBS (30 °C) than in water (35 °C) (Supplementary Information Fig S4c and S4d). The slightly different behavior between PBS and water might be due to a change in the hydration state of the copolymer chains. With higher ionic strength, the copolymer is more readily solubilized. Nevertheless, since the thermoresponsiveness of the copolymer relies on reversible hydrogen bonds between the different copolymer chains, this property is maintained even at higher ionic strength, which represents a strong advantage for use in a biological context as compared with charged or zwitterionic UCST-type (co)polymers [35].

The influence of the AN content on thermoresponsiveness was then assessed directly on the P(AAm-*co*-AN)-*b*-POEGMA diblock copolymers (**P1** to **P8**). The $T_{t\text{-}UCST}$ of the copolymers increased with increasing AN content (Fig. 3a and 3b). The trend was not clearly defined due to the IR measurements of the AN content in the polymers being not precise enough. For 40 mol.% AN (**P8**), the copolymer was insoluble in water at any temperature. While the copolymers had different M_n values ranging between 25 and 82 kg mol^{-1}, this parameter did not appear to have as much impact as the AN content.

3.2. Nanoparticle formulation

As the different copolymers were only soluble in DMSO, which is a water-miscible solvent, the nanoparticles were thus prepared by the nanoprecipitation technique [36]. The average diameters and polydispersity indexes of the obtained nanoparticles in water followed a decreasing trend as the $T_{t\text{-}UCST}$ increased (Fig. 3c). This can be attributed to the different hydration state of the copolymers depending on the temperature of the solution. All formulations were prepared at room temperature (circa 23 °C) and measured at 20 °C. For the copolymer having a $T_{t\text{-}UCST}$ at 30 °C (**P1**), the DLS measurements were not appropriate as the obtained suspension was on the micron size range. While $T_{t\text{-}UCST}$ of **P1** was measured at 30 °C, the onset temperature is lower, close to 20 °C. The copolymer chains were thus hydrated and the nanoparticles swollen. As the $T_{t\text{-}UCST}$ increased, so did the hydrophobicity of the copolymer, which in turn hindered the interactions between water molecules and the copolymer chains thus yielding more compact nanoparticles. The trend reached a lower point at 154 nm with 0.09 as a PdI for **P8**.

Formulation of the thermoresponsive copolymers into nanoparticles in different aqueous media modified their physico-chemical properties. For instance, **P6** led to nanoparticles with a greater average diameter in PBS than in water (Supplementary Information Fig. S5a), revealing a higher hydration state in such a medium. This result is well-correlated with the UCST behavior as the temperature onset for thermoresponsiveness was lower in PBS than in water. DLS measurements were also carried out at 37 °C for **P2** nanoparticles formulated in water (Supplementary Information Fig. S5b). The swelling behavior was observed here once again, as the copolymer chains preferentially interacted with water molecules at higher temperature. This result was indicative of the solubilization mechanism of the nanoparticles as they appeared to swell to bigger sizes before eventually becoming fully soluble at a temperature higher than the $T_{t\text{-}UCST}$.

As for the morphology of the different nanoparticles, TEM images suggested a significant influence of the copolymer's $T_{t\text{-}UCST}$ (Fig. 4). Indeed, for a high $T_{t\text{-}UCST}$ (**P7**), the nano-objects appeared to be well-defined spheres whereas at a lower $T_{t\text{-}UCST}$ (**P2**), the suspension was not homogeneous, and the nano-objects seemed to be fused together in ill-defined shapes. A compromise was made in terms of selection of the polymer for further drug encapsulation studies, as **P2** offered the best choice in terms of $T_{t\text{-}UCST}$ but formed particles larger than 300 nm. The subsequent studies were carried out with **P2**.

3.3. Impact of doxorubicin loading on the nanoparticle properties

Doxorubicin hydrochloride is a water-soluble anticancer drug

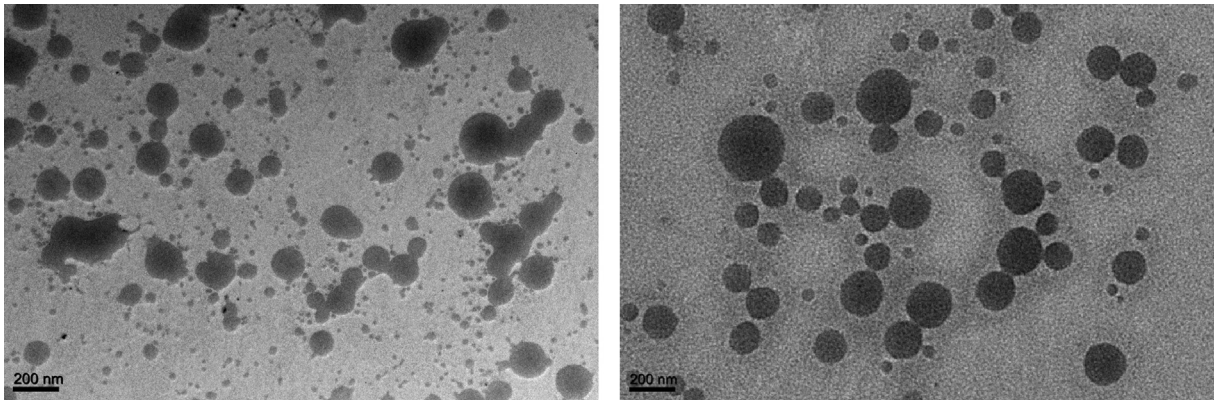

Fig. 4. TEM images of **P2** unloaded nanoparticles (left), **P7** unloaded nanoparticles (right).

widely used to treat a variety of cancers. Here, Dox was rendered hydrophobic by letting it react with triethylamine (weak base) [23,27]. It will therefore be encapsulated in the P(AAm-*co*-AN) hydrophobic core of nanoparticles. We studied the impact of Dox loading on the physico-chemical properties of the nanoparticles. Note that nanoparticles were formulated in water, as formulation in PBS resulted in precipitation of Dox.

The drug loading of Dox showed a linear increase as a function of the initial amount of Dox up to 3.3 mg of initial Dox where the DL value stabilized at around 4 wt% (Fig. 5a). Interestingly, this maximum DL value was in agreement with other studies where Dox was encapsulated in regular non-thermoresponsive polymer nanoparticles [37,38]. Above this maximum value, the copolymer matrix was saturated with Dox and was not able to incorporate more drug. This effect was clearly supported by looking at the encapsulation efficiency, which increased from 30 to 50 wt% as the initial Dox mass increased, and then decreased after saturation of the copolymer matrix (Fig. 5b). Encapsulation of Dox also modified the size and surface charge properties of the nanoparticles as shown in Fig. 5c and 5d. The size followed a decreasing trend as encapsulated Dox increased, and the surface zeta-potential (ζ) became significantly more negative in the presence of Dox compared to unloaded nanoparticles, likely because of the deprotonated state of Dox. The change in surface charge was also indicative of the encapsulation of the drug in the polymer matrix. As for the size decrease of the nanoparticles, it may be due to a preferential interaction between Dox and the copolymer chains, where Dox acted as a hydrophobic nucleus facilitating the formation of more compact and dense nanoparticles.

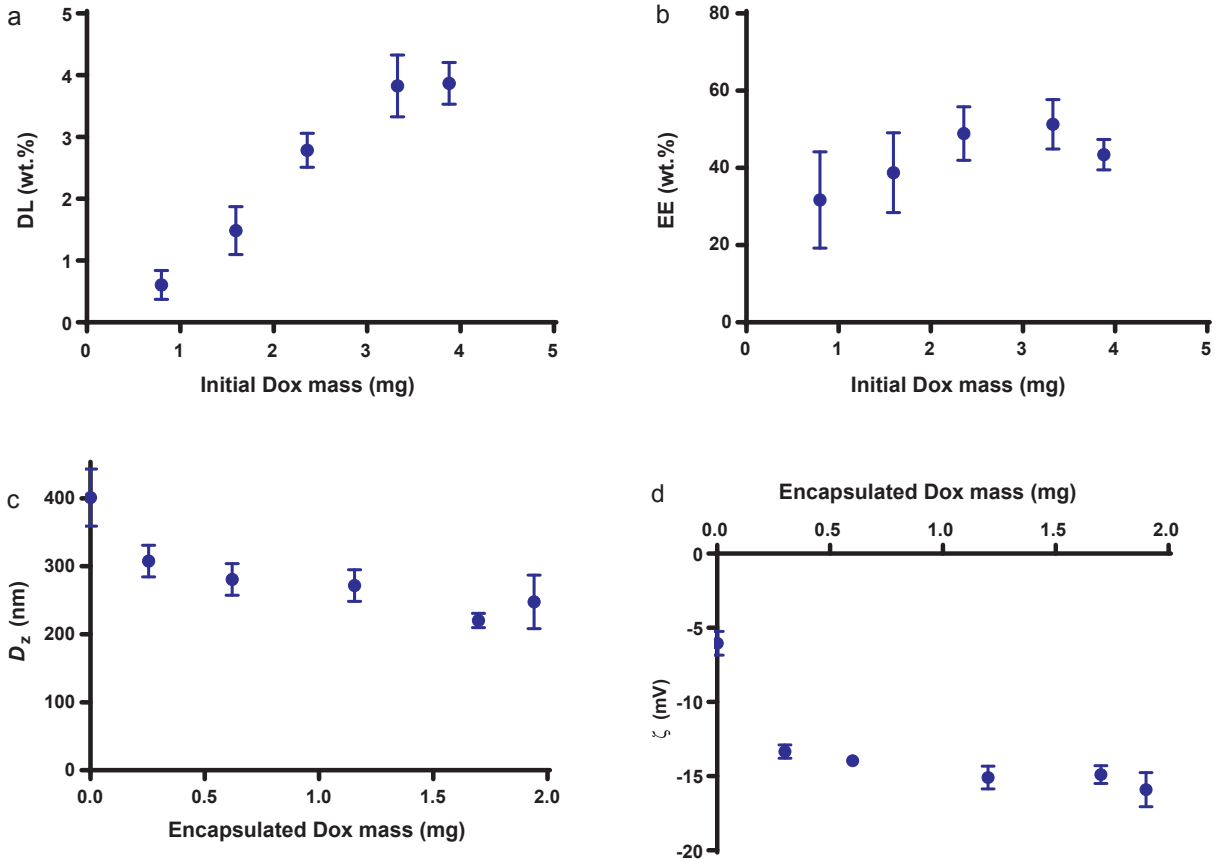

Fig. 5. Physico-chemical properties of Dox loaded NPs formulated with **P2** at 4.5 mg mL^{-1} polymer concentration in water. (a) Drug loading content (DL) and (b) encapsulation efficiency (EE) as a function of initial mass of doxorubicin. (c) D_z and (d) ζ-potential values as a function of encapsulated Dox ($n \geq 2$).

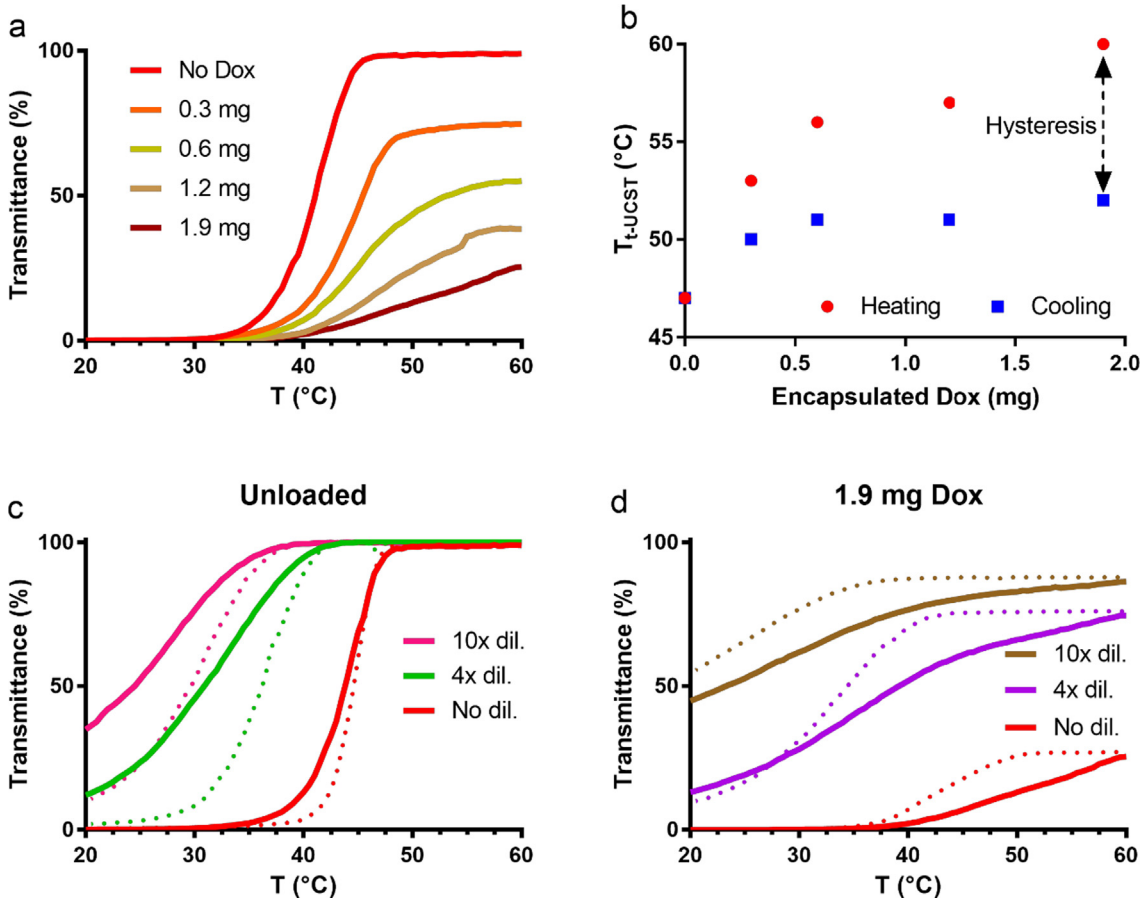

Fig. 6. Doxorubicin encapsulation impact on $T_{t\text{-}UCST}$ of formulated nanoparticles from **P2** at 4.5 mg mL^{-1} in water. (a) Heating transmittance curves with various amounts of encapsulated Dox. (b) Heating and cooling $T_{t\text{-}UCST}$ values depending on the amount of encapsulated Dox. Cooling curves in Supplementary Information Fig. S8. (c) Transmittance curves of unloaded **P2** nanoparticles at 4.5 mg mL^{-1} (red), 4x dilution (green) and 10x dilution (pink) in water. (c) Transmittance curves of Dox-loaded **P2** nanoparticles at 4.5 mg mL^{-1} (red), 4x dilution (purple) and 10x dilution (brown) in water. Lines represent heating transmittance curves; dotted lines represent cooling transmittance curves.

Upon increasing the amount of encapsulated Dox in the nanoparticles, the $T_{t\text{-}UCST}$ increased both for the heating curve (Fig. 6a) and the cooling curve (Fig. 6b). The maximum transmittance value of the nanoparticles containing Dox did not reach 100% due to the presence of Dox that absorbed part of the incoming light even at a high wavelength (600 nm). The maximum transmittance value decreased with increasing the Dox content. The change in $T_{t\text{-}UCST}$ for the heating and cooling curves showed an increase of the hysteresis of the system with increasing the encapsulated Dox content (Fig. 6b). In agreement with our hypothesis, the hysteresis might be due to the strong interaction between Dox and the copolymer chains, resulting in more energy needed to disrupt the Dox-copolymer interactions and fully solubilize the copolymer chains in water. The cooling $T_{t\text{-}UCST}$ values, while higher than that obtained for unloaded nanoparticles, remained constant for the different amounts of encapsulated Dox. This observation can be attributed to the drug release: once Dox was freed from the nanoparticles, the $T_{t\text{-}UCST}$ came back to a value closer to that of the unloaded nanoparticles.

Thermoresponsive copolymers exhibited a phase diagram in aqueous medium that displayed a concentration-dependent cloud point. This aspect must be elucidated to verify if the thermoresponsive properties of the nanoparticle formulation at 4.5 mg mL^{-1} of copolymer remained similar upon dilution, which is an important feature for the applicability. Dilution decreased the $T_{t\text{-}UCST}$ of the suspensions even in the presence of Dox (Fig. 6c and d). While the thermoresponsiveness was retained, a shift of the $T_{t\text{-}UCST}$ towards lower values was observed; from 47 °C down to 40 °C in the case of unloaded nanoparticles (Fig. 6c). Not only did the $T_{t\text{-}UCST}$ decrease but also the onset temperature; from 30 °C to below 20 °C. For Dox-loaded nanoparticles, this phenomenon was still observed (Fig. 6d). For the cooling $T_{t\text{-}UCST}$ values, they were equal to 51, 42 and 37 °C for undiluted, 4 times diluted and 10 times diluted suspensions, respectively. This change of $T_{t\text{-}UCST}$ upon dilution raised questions regarding the applicability of this system for clinical use. Indeed, once administered to the patient intravenously, the formulation undergoes an important dilution, from a 500 mL perfusion bag to a 5-liter blood volume. This issue may be tackled by heating the tumor at mild-hyperthermia prior to the administration of the formulation, to minimize the chance of uncontrolled drug release.

Upon Dox loading, the overall shape of the nanoparticles visible by TEM did not change conversely to the size which appeared to be smaller (Supplementary Information, Fig. S6), which is in agreement with DLS measurements. Traditional polymer nanoparticles made from amphiphilic diblock copolymers, such as PLA-*b*-PEG, exhibit a well-defined spherical shape. Solubility of P(AAm-*co*-AN)-*b*-POEGMA in water is temperature- and concentration-dependent unlike PLA-*b*-PEG. Thus, our hypothesis is that in observation conditions, as nanoparticles are diluted to allow observation, some copolymer chains were solubilized and allowed merging of different nanoparticles to form ill-defined objects.

3.4. Cell culture

The aim of the cell culture studies was to show an enhanced activity of Dox encapsulated in nanoparticles under mild hyperthermia

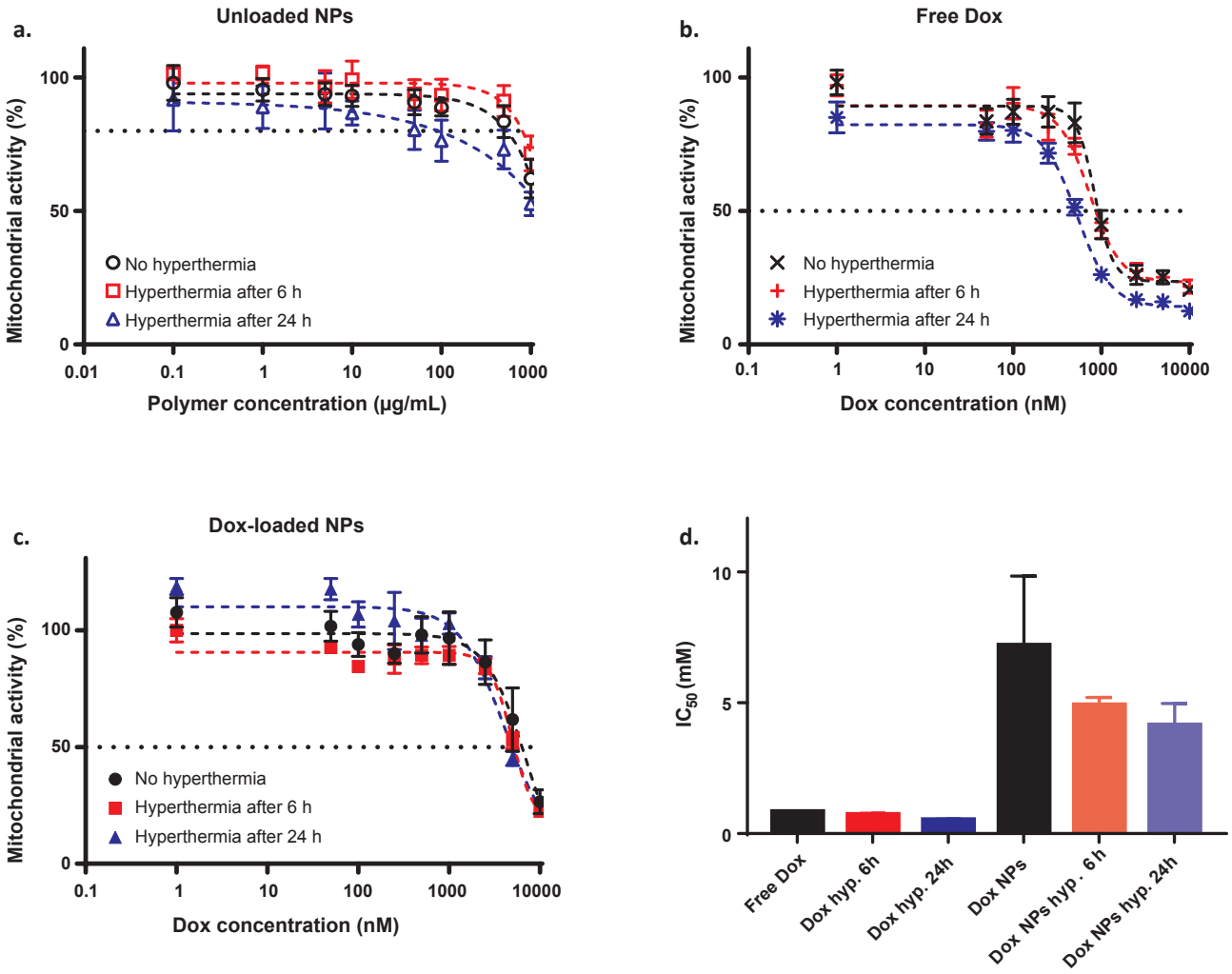

Fig. 7. Mitochondrial activity of OVCAR-3 cells in the presence of unloaded **P2** nanoparticles (a), free Dox (b), or Dox-loaded **P2** nanoparticles (c) ± hyperthermia (43 °C). For unloaded nanoparticles, dashed line indicates 80% mitochondrial activity, for others dashed line indicates the IC_{50} (d).

conditions. OVCAR-3 cells were chosen as they are Dox-sensitive and represent a good cancer model for localized hyperthermia [39,40]. The mitochondrial activity results showed that unloaded nanoparticles were not toxic up to 500 µg mL^{-1}, whereas 60% of mitochondrial activity was retained at 1 mg mL^{-1} (Fig. 7a). This result was encouraging as it showed that the thermoresponsive copolymer used is rather well-tolerated making it a good candidate for drug delivery applications.

Mild hyperthermia was applied for 30 min, at 6 h or 24 h post-treatment. The trend showed that cytotoxicity was greater when hyperthermia was applied 24 h post-treatment rather than 6 h post-treatment (Fig. 7). This trend was verified in the case of free Dox and for Dox-loaded nanoparticles although not statistically significant. IC_{50} for free Dox was at 0.8 mM, whereas the IC_{50} for Dox-loaded nanoparticles was at 7.2 mM (Fig. 7d). The increase of the IC_{50} was due to the encapsulation of the drug in the nanoparticles, where it is rendered less accessible to the cells. Dox induced its anticancer activity inside the cells' nucleus where it intercalates between complementary DNA strands, inhibiting the progression of topoisomerase II and further blocking proper transcription and replication [41]. This mechanism of action thus requires Dox to reach the cells' nucleus and not only reside in the cytosol for it to exert its anticancer activity. In the results shown here, the 5-fold difference between free Dox and encapsulated Dox is significant and might be due to the strong affinity between the copolymer and Dox mentioned earlier in the manuscript. Indeed, if Dox has a strong affinity with the copolymer, it may not readily be released from the nanoparticles and reach the cell's nucleus, as it might be retained by the copolymer, which has a large molar mass not allowing proper diffusion to the cell's nucleus. However, upon hyperthermia, the polymer chains should be solubilized, allowing Dox to freely diffuse away from the copolymer. As our results under hyperthermia showed that $T_{t\text{-}UCST}$ of Dox-loaded nanoparticles decreased upon dilution, we expected to see a difference between unheated and heated nanoparticles. While there was a visible trend, we were not able to obtain the same activity, i.e. same IC_{50}, as the free Dox when treating with Dox-loaded nanoparticles with hyperthermia.

Several aspects of the system can be improved to address some of the limitations presented in this study. Regarding the dilution affecting the UCST, a possible solution would be to add a hydrophobic block to the polymer that would act as a solid foundation upon which the nanoparticles could be built. This would force the thermoresponsive copolymer chains to remain close to each other at any dilution. On the contrary, this solution may also force the drug to be primarily encapsulated in the hydrophobic polymer chains, thus having potentially less drug release upon heating. Nevertheless, this methodology is already extensively used for LCST-type drug delivery systems and would be interesting to test for UCST-type drug delivery systems. The nature of the encapsulated anticancer drug can also be changed to select a molecule whose anticancer mechanism takes place inside the cell's cytosol as opposed to its nucleus. For instance, taxane derivatives such as paclitaxel are good candidates as they disrupt the microtubules' stability

in the cytosol. In terms of physico-chemistry, these drugs are already hydrophobic, simplifying the preparation of the drug-loaded nanoparticles.

4. Conclusion

The aim of this study was to formulate thermoresponsive nanoparticles from P(AAm-*co*-AN), a hydrogen bonding-based UCST copolymer building block. We successfully synthesized UCST-type P(AAm-*co*-AN)-*b*-POEGMA diblock copolymer by a two-step RAFT polymerization and successfully tuned the thermoresponsiveness by varying the amount of AN in the copolymer. The copolymer was formulated into nanoparticles by the nanoprecipitation technique into stable nanoparticles of different sizes and dispersity governed by the $T_{t\text{-}UCST}$ of the copolymer: the higher the $T_{t\text{-}UCST}$, the smaller the size. Encapsulation of Dox was achieved and modified the properties of the nanoparticles in a way never reported before. Surprisingly, the higher the amount of encapsulated Dox, the higher the $T_{t\text{-}UCST}$ of the nanoparticles. In vitro, unloaded nanoparticles were not toxic up to 500 μg mL^{-1}. However, the effect of hyperthermia on cell viability was not significant probably due to the modification of $T_{t\text{-}UCST}$ of the nanoparticles upon dilution. The system can still be improved by changing the encapsulated drug or adding a hydrophobic polymer block to yield a better-defined suspension less sensitive to dilution effects. Taken together, these results highlighted the crucial role of the drug encapsulation and dilution on the expected beneficial effect of the thermoresponsiveness. Therefore, it seems important to carefully study those parameters for any kind of thermosensitive nanoscale drug delivery systems.

Acknowledgements

Authors acknowledge the support of la Ligue contre le Cancer for Alexandre Bordat's Ph.D. fellowship, Cancéropôle IDF Emergence and Fondation ARC for funding. The present work has benefited also from the core facilities of Imagerie-Gif, (http://www.i2bc.paris-saclay.fr), member of IBiSA (http://www.ibisa.net), supported by "France-BioImaging" (ANR-10-INBS-04-01), and the Labex "Saclay Plant Science" (ANR-11-IDEX-0003-02). Institut Galien Paris-Sud is a member of the Laboratory of Excellence LERMIT supported by a grant from ANR (ANR-10-LABX-33). Authors would like to acknowledge the precious help of S. Denis for cell culture and C. Dejean for NMR.

Appendix A. Supplementary material

Supplementary data to this article can be found online at https://doi.org/10.1016/j.ejpb.2019.07.001.

References

[1] D.E. Owens, N.A. Peppas, Opsonization, biodistribution, and pharmacokinetics of polymeric nanoparticles, Int. J. Pharm. 307 (2006) 93–102, https://doi.org/10.1016/J.IJPHARM.2005.10.010.
[2] M.E.R. O'Brien, N. Wigler, M. Inbar, R. Rosso, E. Grischke, A. Santoro, R. Catane, D. Kieback, G.P. Tomczak, S. Ackland, P.F. Orlandi, L. Mellars, L. Alland, C. Tendler, Reduced cardiotoxicity and comparable efficacy in a phase III trial of pegylated liposomal doxorubicin HCl (CAELYX™/Doxil®) versus conventional doxorubicin for first-line treatment of metastatic breast cancer, Ann. Oncol. 15 (2004) 440–449, https://doi.org/10.1093/annonc/mdh097.
[3] S. Mura, J. Nicolas, P. Couvreur, Stimuli-responsive nanocarriers for drug delivery, Nat. Mater. 12 (2013) 991–1003, https://doi.org/10.1038/nmat3776.
[4] T. Boissenot, A. Bordat, E. Fattal, N. Tsapis, Ultrasound-triggered drug delivery for cancer treatment using drug delivery systems: From theoretical considerations to practical applications, J. Control. Release. 241 (2016) 144–163, https://doi.org/10.1016/j.jconrel.2016.09.026.
[5] D.E. Kruse, Chun-Yen Lai, D.N. Stephens, P. Sutcliffe, E.E. Paoli, S.H. Barnes, K.W. Ferrara, Spatial and temporal-controlled tissue heating on a modified clinical ultrasound scanner for generating mild hyperthermia in tumors, IEEE Trans. Biomed. Eng. 57 (2010) 155–166, https://doi.org/10.1109/TBME.2009.2029703.
[6] J.E. Johnson, P.F. Maccarini, D. Neuman, P.R. Stauffer, Automatic temperature controller for multielement array hyperthermia systems, IEEE Trans. Biomed. Eng. 53 (2006) 1006–1015, https://doi.org/10.1109/TBME.2006.873559.
[7] Y. Nagata, M. Hiraoka, Y. Nishimura, S. Masunaga, M. Mitumori, Y. Okuno, M. Fujishiro, S. Kanamori, N. Horii, K. Akuta, K. Sasai, M. Abe, Y. Fukuda, Clinical results of radiofrequency hyperthermia for malignant liver tumors, Int. J. Radiat. Oncol. Biol. Phys. 38 (1997) 359–365, https://doi.org/10.1016/S0360-3016(96)00625-6.
[8] G. Hoffmann, Principles and working mechanisms of water-filtered infrared-A (wIRA) in relation to wound healing, GMS Krankenhhyg. Interdiszip. 2 (2007).
[9] G. Kong, R.D. Braun, M.W. Dewhirst, Hyperthermia enables tumor-specific nanoparticle delivery: effect of particle size, Cancer Res. 60 (2000) 4440 LP – 4445.
[10] G. Kong, R.D. Braun, M.W. Dewhirst, Characterization of the effect of hyperthermia on nanoparticle extravasation from tumor vasculature, Cancer Res. 61 (2001) 3027 LP – 3032.
[11] S.K. Calderwood, J.R. Theriault, J. Gong, How is the immune response affected by hyperthermia and heat shock proteins? Int. J. Hyperth. 21 (2005) 713–716, https://doi.org/10.1080/02656730500340794.
[12] B. Hildebrandt, P. Wust, O. Ahlers, A. Dieing, G. Sreenivasa, T. Kerner, R. Felix, H. Riess, The cellular and molecular basis of hyperthermia, Crit. Rev. Oncol. Hematol. 43 (2002) 33–56, https://doi.org/10.1016/S1040-8428(01)00179-2.
[13] M. Dunne, K. Hynynen, C. Allen, Thermosensitive nanomedicines could revolutionize thermal therapy in oncology, Nano Today. 16 (2017) 9–13, https://doi.org/10.1016/j.nantod.2017.08.001.
[14] T. Ta, T.M. Porter, Thermosensitive liposomes for localized delivery and triggered release of chemotherapy, J. Control. Release. 169 (2013) 112–125, https://doi.org/10.1016/j.jconrel.2013.03.036.
[15] M.C. Sandström, L.M. Ickenstein, L.D. Mayer, K. Edwards, Effects of lipid segregation and lysolipid dissociation on drug release from thermosensitive liposomes, J. Control. Release. 107 (2005) 131–142, https://doi.org/10.1016/J.JCONREL.2005.06.001.
[16] B. Banno, L.M. Ickenstein, G.N.C. Chiu, M.B. Bally, J. Thewalt, E. Brief, E.K. Wasan, The functional roles of poly(ethylene glycol)-lipid and lysolipid in the drug retention and release from lysolipid-containing thermosensitive liposomes in vitro and in vivo, J. Pharm. Sci. 99 (2010) 2295–2308, https://doi.org/10.1002/JPS.21988.
[17] S. Cammas, K. Suzuki, C. Sone, Y. Sakurai, K. Kataoka, T. Okano, Thermo-responsive polymer nanoparticles with a core-shell micelle structure as site-specific drug carriers, J. Control. Release. 48 (1997) 157–164, https://doi.org/10.1016/S0168-3659(97)00040-0.
[18] M. Karimi, P. Sahandi Zangabad, A. Ghasemi, M. Amiri, M. Bahrami, H. Malekzad, H. Ghahramanzadeh Asl, Z. Mahdieh, M. Bozorgomid, A. Ghasemi, M.R. Rahmani Taji Boyuk, M.R. Hamblin, Temperature-responsive smart nanocarriers for delivery of therapeutic agents: applications and recent advances, ACS Appl. Mater. Interfaces 8 (2016) 21107–21133, https://doi.org/10.1021/acsami.6b00371.
[19] J. Seuring, S. Agarwal, First example of a universal and cost-effective approach: polymers with tunable upper critical solution temperature in water and electrolyte solution, Macromolecules 45 (2012) 3910–3918.
[20] F. Käfer, F. Liu, U. Stahlschmidt, V. Jérôme, R. Freitag, M. Karg, S. Agarwal, LCST and UCST in one: double thermoresponsive behavior of block copolymers of poly (ethylene glycol) and poly(acrylamide-co-acrylonitrile), Langmuir 31 (2015) 8940–8946, https://doi.org/10.1021/acs.langmuir.5b02006.
[21] L. Hou, P. Wu, Understanding the UCST-type transition of P(AAm-co-AN) in H_2O and D_2O: dramatic effects of solvent isotopes, Soft Matter. 11 (2015) 7059–7065, https://doi.org/10.1039/C5SM01745A.
[22] H. Zhang, X. Tong, Y. Zhao, Diverse thermoresponsive behaviors of uncharged UCST block copolymer micelles in physiological medium, Langmuir 30 (2014) 11433–11441, https://doi.org/10.1021/la5026334.
[23] G. Huang, H. Li, S.T. Feng, X. Li, G. Tong, J. Liu, C. Quan, Q. Jiang, C. Zhang, Z. Li, Self-assembled UCST-type micelles as potential drug carriers for cancer therapeutics, Macromol. Chem. Phys. 216 (2015) 1014–1023, https://doi.org/10.1002/macp.201400546.
[24] A. Asadujjaman, A. Bertin, A. Schönhals, Dielectric analysis of the upper critical solution temperature behaviour of a poly(acrylamide-co-acrylonitrile) copolymer system in water, Soft Matter. 13 (2017) 2384–2393, https://doi.org/10.1039/C6SM02684B.
[25] A. Asadujjaman, B. Kent, A. Bertin, Phase transition and aggregation behaviour of an UCST-type copolymer poly(acrylamide-co-acrylonitrile) in water: effect of acrylonitrile content, concentration in solution, copolymer chain length and presence of electrolyte, Soft Matter. 13 (2017) 658–669, https://doi.org/10.1039/C6SM02262F.
[26] J. Yang, S. Zhai, H. Qin, H. Yan, D. Xing, X. Hu, NIR-controlled morphology transformation and pulsatile drug delivery based on multifunctional phototheranostic nanoparticles for photoacoustic imaging-guided photothermal-chemotherapy, Biomaterials 176 (2018) 1–12, https://doi.org/10.1016/J.BIOMATERIALS.2018.05.033.
[27] W. Li, L. Huang, X. Ying, Y. Jian, Y. Hong, F. Hu, Y. Du, Antitumor drug delivery modulated by a polymeric micelle with an upper critical solution temperature, Angew. Chemie Int. Ed. 54 (2015) 3126–3131, https://doi.org/10.1002/anie.201411524.
[28] B.Y.K. Chong, T.P.T. Le, G. Moad, E. Rizzardo, S.H. Thang, More versatile route to block copolymers and other polymers of complex architecture by living radical polymerization: the RAFT process, Macromolecules 32 (1999) 2071–2074, https://doi.org/10.1021/ma981472p.
[29] G. Moad, J. Chiefari, Y.K. Chong, J. Krstina, R.T. Mayadunne, A. Postma, E. Rizzardo, S.H. Thang, Living free radical polymerization with reversible addition - fragmentation chain transfer (the life of RAFT), Polym. Int. 49 (2000) 993–1001, https://doi.org/10.1002/1097-0126(200009)49:9<993::AID-PI506>3.0.CO;2-6.
[30] C. Tang, T. Kowalewski, K. Matyjaszewski, RAFT polymerization of acrylonitrile and preparation of block copolymers using 2-cyanoethyl dithiobenzoate as the

transfer agent, Macromolecules 36 (2003) 8587–8589, https://doi.org/10.1021/ma034942a.
[31] D.B. Thomas, A.J. Convertine, L.J. Myrick, C.W. Scales, A.E. Smith, A.B. Lowe, Y.A. Vasilieva, N. Ayres, C.L. McCormick, Kinetics and molecular weight control of the polymerization of acrylamide via RAFT, Macromolecules 37 (2004) 8941–8950, https://doi.org/10.1021/ma048199d.
[32] H. Otsuka, Y. Nagasaki, K. Kataoka, PEGylated nanoparticles for biological and pharmaceutical applications, Adv. Drug Deliv. Rev. 64 (2012) 246–255, https://doi.org/10.1016/J.ADDR.2012.09.022.
[33] F.M. Veronese, P. Caliceti, O. Schiavon, Branched and linear poly(ethylene glycol): Influence of the polymer structure on enzymological, pharmacokinetic, and immunological properties of protein conjugates, J. Bioact. Compat. Polym. 12 (1997) 196–207, https://doi.org/10.1177/088391159701200303.
[34] J.-F. Lutz, Polymerization of oligo(ethylene glycol) (meth)acrylates: Toward new generations of smart biocompatible materials, J. Polym. Sci. Part A Polym. Chem. 46 (2008) 3459–3470, https://doi.org/10.1002/pola.22706.
[35] J. Seuring, S. Agarwal, Polymers with upper critical solution temperature in aqueous solution, Macromol. Rapid Commun. 33 (2012) 1898–1920, https://doi.org/10.1002/marc.201200433.
[36] H. Fessi, F. Puisieux, J.P. Devissaguet, N. Ammoury, S. Benita, Nanocapsule formation by interfacial polymer deposition following solvent displacement, Int. J. Pharm. 55 (1989) R1–R4, https://doi.org/10.1016/0378-5173(89)90281-0.
[37] T. Betancourt, B. Brown, L. Brannon-Peppas, Doxorubicin-loaded PLGA nanoparticles by nanoprecipitation: preparation, characterization and *in vitro* evaluation, Nanomedicine 2 (2007) 219–232, https://doi.org/10.2217/17435889.2.2.219.
[38] J. Park, P.M. Fong, J. Lu, K.S. Russell, C.J. Booth, W.M. Saltzman, T.M. Fahmy, PEGylated PLGA nanoparticles for the improved delivery of doxorubicin, Nanomed. Nanotechnol. Biol. Med. 5 (2009) 410–418, https://doi.org/10.1016/j.nano.2009.02.002.
[39] S.-W. Wang, X.-Y. He, M.-Z. Li, High-intensity focused ultrasound compared with irradiation for ovarian castration in premenopausal females with hormone receptor-positive breast cancer after radical mastectomy, Oncol. Lett. 4 (2012) 1087–1091, https://doi.org/10.3892/ol.2012.860.
[40] H. He, T. Yu, Y. Zhang, The Interaction between a drug and ultrasound in sonochemotherapy against ovarian cancers, Ultraschall Der Medizin – Eur. J. Ultrasound. 33 (2010) 275–282, https://doi.org/10.1055/s-0029-1245876.
[41] A. Bodley, L.F. Liu, M. Israel, R. Seshadri, Y. Koseki, F.C. Giuliani, S. Kirschenbaum, R. Silber, M. Potmesil, DNA topoisomerase II-mediated interaction of doxorubicin and daunorubicin congeners with DNA, Cancer Res. 49 (1989) 5969–5978.